Current Applied Physics 11 (2011) S110–S119

Contents lists available at ScienceDirect

Current Applied Physics

journal homepage: www.elsevier.com/locate/cap

Microstructures and electrical properties of lead-based PBZNZT and lead-free BNKT piezoelectric ceramics using microwave sintering

P.Y. Chen [a,*], C.S. Chen [b], C.C. Chou [c], T.Y. Tseng [d], H.D. Chen [e]

[a] Department of Mechanical Engineering, Ming-Chi University of Technology, Taipei 24301, Taiwan, ROC
[b] Department of Mechanical Engineering, Hwa-Hsia Institute of Technology, Taipei 235, Taiwan, ROC
[c] Department of Mechanical Engineering, National Taiwan University of Science and Technology, Taipei 10672, Taiwan, ROC
[d] Department of Electronics Engineering & Institute of Electronics, National Chiao-Tung University, Hsinchu 300, Taiwan, ROC
[e] Department of Physics, Tunghai University, Taichung 407, Taiwan, ROC

ARTICLE INFO

Article history:
Received 23 June 2010
Received in revised form
14 February 2011
Accepted 14 March 2011
Available online 2 April 2011

Keywords:
Microwave sintering
Lead-free ceramics
Ferroelectric
Piezoelectric
Microstructures
Electrical properties

ABSTRACT

This paper is a comparative study involving sintering conditions (different sintering temperatures and time), process (conventional and microwave sintering), microstructures, and electrical measurements to investigate the mechanism of microwave absorption, and the difference in the microstructural characteristics and electrical properties of lead-based and lead-free ceramics. The lead-based piezoelectric ceramics are $x(0.94PbZn_{1/3}Nb_{2/3}O_3 + 0.06BaTiO_3) + (1-x)PbZr_yTi_{1-y}O_3$ where $x = 0.5$, $y = 0.52$ (abbreviated as PBZNZT) and the lead-free ceramics are $(Bi_{0.5}(Na_{1-x}K_x)_{0.5})TiO_3$ where $x = 0.18$ (abbreviated as BNKT), all sintered by microwave heating. Experimental results indicate that PBZNZT and BNKT specimens have different microwave absorption efficiencies. Compared with BNKT samples, PBZNZT samples absorb microwave radiation more efficiently in MWS process. This might be attributed to the contribution of the dielectric constant and dipole loss which might dominate the absorption of microwave energy for ferroelectric and piezoelectric materials. HRTEM and energy dispersive spectroscopic investigations show that the grain boundaries of MWS samples exhibit less PbO and ZnO segregation than those of CS samples form PBZNZT specimens. On the other hand, BNKT specimens exhibit no compositional segregation at the grain boundaries after the CS and MWS processes. In addition, the MWS process can achieve a more uniform composition and crystallization in PBZNZT and BNKT ceramics, thus improving the electrical properties.

1. Introduction

In recent years, lead zirconate titanate–lead zinc niobate $(Pb(Zr_{1/2}Ti_{1/2})O_3–Pb(Zn_{1/3}Nb_{2/3})O_3$ (PZT–PZN) piezoelectric materials have had wide applications in piezoelectric actuators, sensors, and transducers due to their high dielectric, piezoelectric, and ferroelectric properties [1–3]. However, Perovskite PZN has been reported to be thermodynamically unstable over the wide temperature range of 600–1400 °C [4]. A useful method to stabilize the perovskite structure is to add additives such as BaTiO3 (BT), SrTiO3 (ST) and others. For example, a slight increase in the amount of BT stabilizes PZN [5,6], but the phase transformation temperature of PZN may be reduced to below room temperature. Accordingly, other stabilizers must be added to raise the ferroelectric–paraelectric phase transformation temperature. PbTiO3 (PT)–PbZrO3 (PZ) are commonly employed to adjust those properties. However, many countries have recently restricted the use of lead oxide by drafting legislation due to toxicity and its high vapor pressure, which is harmful to people and environment. Therefore, it is necessary and urgent to search for lead-free piezoelectric ceramics with excellent piezoelectric properties [7]. $Bi_{0.5}Na_{0.5}TiO_3$ (BNT) is considered an excellent candidate for lead-free piezoelectric ceramics due to its relatively large remnant polarization ($P_r = 38\ \mu C/cm^2$) and high Curie temperature ($T_c = 320\ °C$) [8–10]. However, BNT has the drawback of high conductivity and a high coercive field E_c, which can cause problems in the poling process [11]. BNT-based solid solutions have been studied and some BNT-based lead-free piezoelectric ceramics systems with superior piezoelectric properties have been reported, such as BNT–$BaTiO_3$, BNT–$Bi_{0.5}K_{0.5}TiO_3$, BNT–$BaTiO_3$–$Bi_{0.5}K_{0.5}TiO_3$, BNT–$(Na,K)NbO_3$, BNT–$Ba(Ti,Zr)O_3$, BNT–$(BiLi)TiO_3$–$Bi_{0.5}K_{0.5}TiO_3$ [12–17] and so on. Among these materials, the excellent piezoelectric and dielectric properties of $(1-x)$ BNT–x BKT systems can be achieved near the rhombohedral–tetragonal morphotropic phase boundary (MPB) with $x = 0.16–0.20$. Because $Bi_{0.5}K_{0.5}TiO_3$ can be partially

* Corresponding author. Tel.: +886 2 29089899x4566; fax: +886 2 29063269.
E-mail address: pinyi@mail.mcut.edu.tw (P.Y. Chen).

1567-1739/$ – see front matter © 2011 Elsevier B.V. All rights reserved.
doi:10.1016/j.cap.2011.03.039

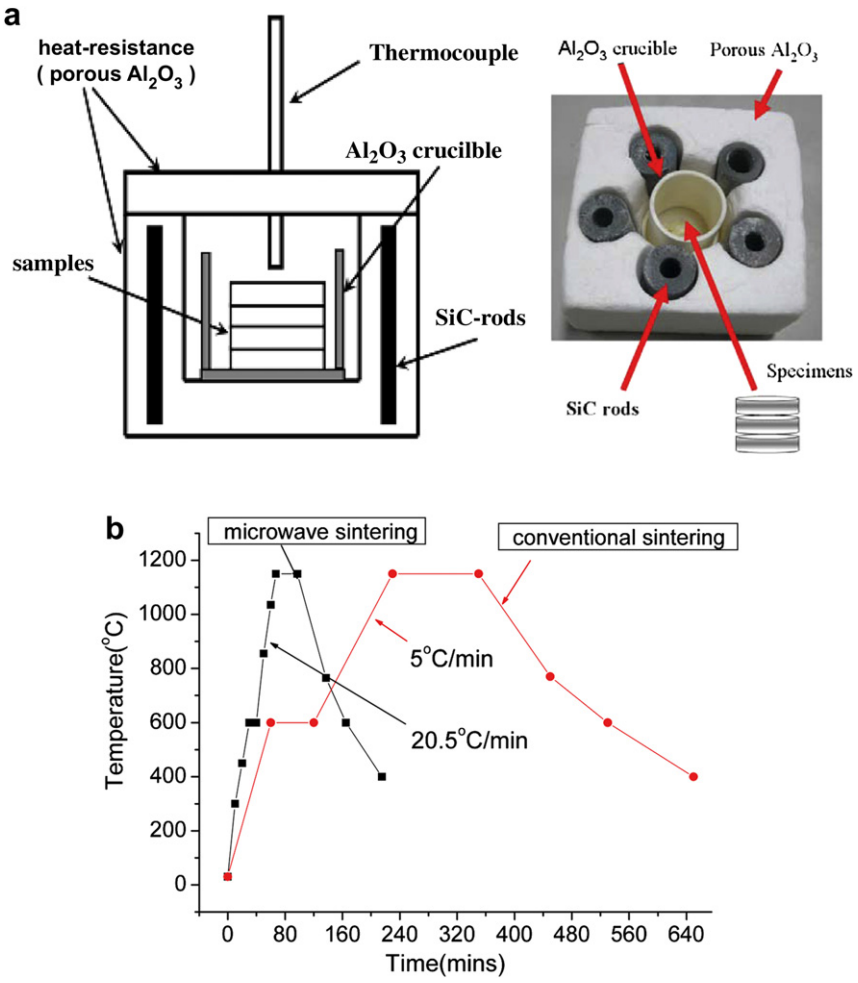

Fig. 1. (a) Microwave hybrid heating structure, and (b) sintering temperature profiles of the CS and the MW processes.

substituted for BNT, E_c can be reduced. Higher values of the electromechanical coupling factor (K_p) and the dielectric constant (ε_r) are observed around the MPB region. Furthermore, a significant problem of BNT-based ceramics is its large leakage current, that is often correlated with the vaporization of Bi during sintering and the subsequent defects forming at high temperatures [18].

Microwave sintering is a special process technique with unique characteristics, such as rapid heating, enhanced densification rate, lower sintering temperature, and lower cost when compared with conventional heating [19–23]. Many investigations have proposed the development of high-performance piezoelectric materials such as $Pb(Zr,Ti)O_3$ (PZT), $PbLa(Zr,Ti)O_3$ (PLZT) using microwave sintering [24–31]. The microwave frequencies of 2.45 and 30 GHz were used in sintering of PZT ceramics, the properties of which were improved by the reduction in PbO volatility [28,29]. Therefore, the microwave sintering technique could be an appropriate approach for improving sintering of easily evaporating elements. On the other hand, electromagnetic waves interact with ceramic materials, leading to volumetric heating through microwave radiation, but the microwave sintering behavior of ceramics depends strongly on

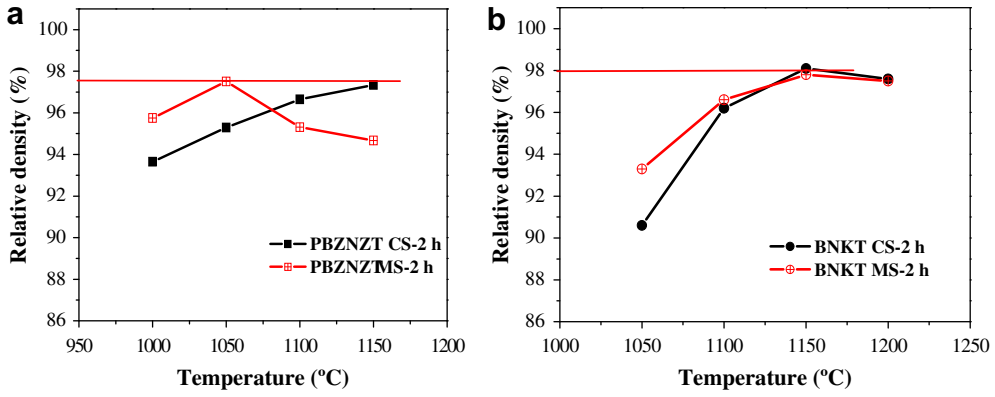

Fig. 2. The relative density of (a) PBZNZT and (b) BNKT ceramics at different sintering temperatures for the CS and MWS processes.

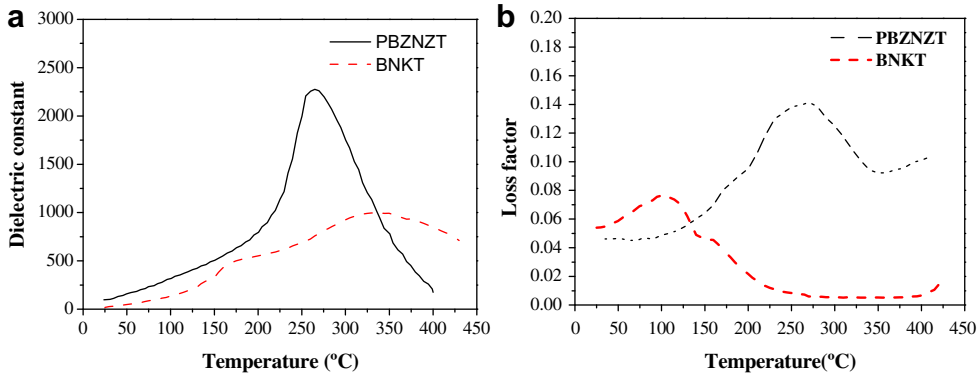

Fig. 3. (a) Dielectric constant and (b) dielectric loss factor were measured at a 2.45 GHz frequency over the range of temperatures from 25 °C to 400 °C.

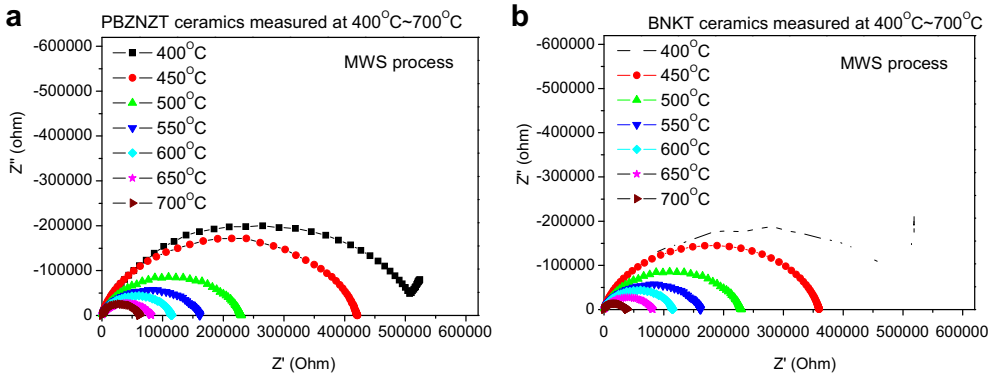

Fig. 4. Conductivity measurements of AC impedance as a function of temperature in (a) PBZNZT and (b) BNKT specimens.

their ability to microwave absorption. Many factors affect the microwave absorption ability of the materials. For example, the microwave power deposited in the materials and microwave penetration depth of the materials play important roles in estimating the microwave absorption ability. The microwave power deposited in the ceramics is given by the following equation:

$$P = \omega \varepsilon_0 \varepsilon_r \tan\delta E_i^2 = 2\pi f \varepsilon_0 \varepsilon_r \tan\delta E_i^2 \quad (1)$$

where E_i is the magnitude of the electric field entering materials, ε_r is the relative dielectric constant, ε_0 is the permittivity of free space; f is the microwave frequency, and tan δ is the dielectric loss factor. In addition, there are two main physical loss mechanisms: the conduction loss and dipole relaxation loss. These losses may be combined into an effective dielectric loss factor. According to Eq. (1), the dielectric properties (dielectric constant and dielectric loss factor) of the materials strongly affect the microwave absorption ability of the ceramics. On the other hand, the interaction between the microwave radiation and the ceramics often changes at different sintering temperatures [32]. For example, Al_2O_3, ZrO_2 and Si_3N_4 have a low absorption ability of microwave radiation at lower temperatures and an increased ability at higher temperatures. To accelerate initial heating at lower temperatures and obtain a more uniform heating, hybrid heat with SiC-rod susceptor was used to aid sintering at lower temperatures.

The microwave process requires specialized sintering engineering, but few studies have been performed on lead-free piezoelectric ceramics to estimate the effect of the microwave process. Therefore, in the present work, two kinds of ceramics, lead-based piezoelectric ceramics $x(0.94PbZn_{1/3}Nb_{2/3}O_3 + 0.06BaTiO_3) + (1-x)$ $PbZr_yTi_{1-y}O_3$ (abbreviated as PBZNZT) and lead-free $(Bi_{0.5}(Na_{1-x}K_x)_{0.5})TiO_3$ piezoelectric ceramics (abbreviated as BNKT), were used to investigate the correlation between the electrical properties and microstructural characteristics of the specimens using microwave sintering when compared with the conventional sintered samples. At the same time, the difference in the coupling microwave energy between the BNKT and PBZNZT ceramics is evaluated to understand the mechanisms of microwave absorption.

2. Experiments

The specimens of $x(0.94PbZn_{1/3}Nb_{2/3}O_3 + 0.06BaTiO_3) + (1-x)$ $PbZr_yTi_{1-y}O_3$ (abbreviated as PBZNZT) with $x = 0.5$ and $y = 0.52$

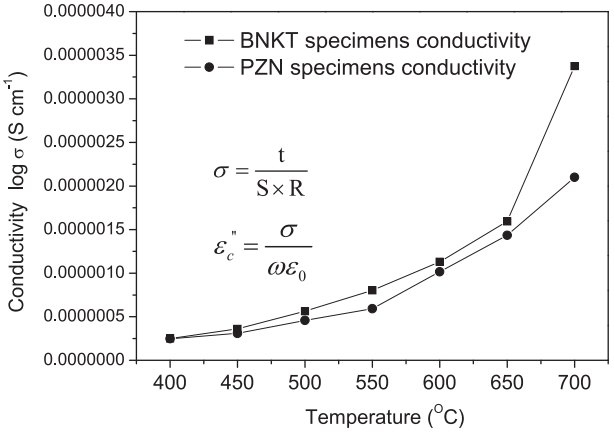

Fig. 5. Conductivity changes with temperature for PBZNZT and BNKT samples using the microwave sintering process.

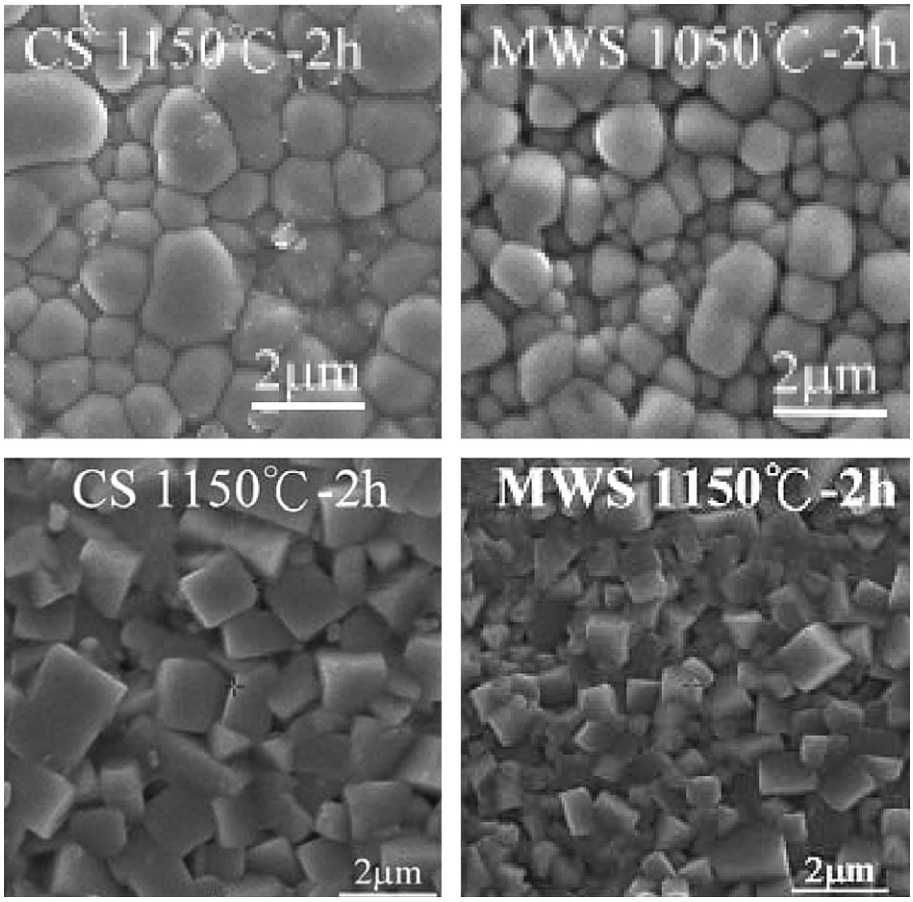

Fig. 6. SEM images of the CS and MWS processes with similar densities for (a), (b) PBZNZT samples and (c), (d) BNKT samples.

were fabricated in this experiment. PbO, ZnO, Nb_2O_5, ZrO_2, $BaCO_3$ and TiO_2 were used as the initial raw materials. The specimens were prepared by an A-site-element sequential mixing columbite (ASMC) method [33,34]. Following calcinations, the ground and ball-milled powders were pressed into discs with a diameter of 10 mm and a thickness of 1 mm. The lead-free $(Bi_{0.5}(Na_{1-x}K_x)_{0.5})TiO_3$ (abbreviated as BNKT) ceramics with $x = 0.18$ were fabricated using a conventional solid state reaction technique. Reagent grade oxide and carbonate powders such as Bi_2O_3, Na_2CO_3, K_2CO_3 and TiO_2 were used as the initial raw materials. All powders were ball milled for 24 h and were calcined at 850 °C for 2 h. The calcined powders were also reground and pressed into disc specimens with a diameter of 10 mm and a thickness of 1 mm. A multimode 2.45 GHz microwave furnace with a power output of 1 kW was used in the microwave sintering process, and the specimens were sintered with temperatures between 1000 and 1150 °C for sintering times ranging from 30 to 120 min. The conventional sintering (CS) process was also performed and sintering conditions were the same as these of the microwave sintering (MWS) process. To prevent the evaporation of elements, PBZNZT specimens used a crucible that contained PbZrO3 powders to prevent the evaporation of PbO, and BNKT specimens were sintered using a crucible that contained calcined BNKT

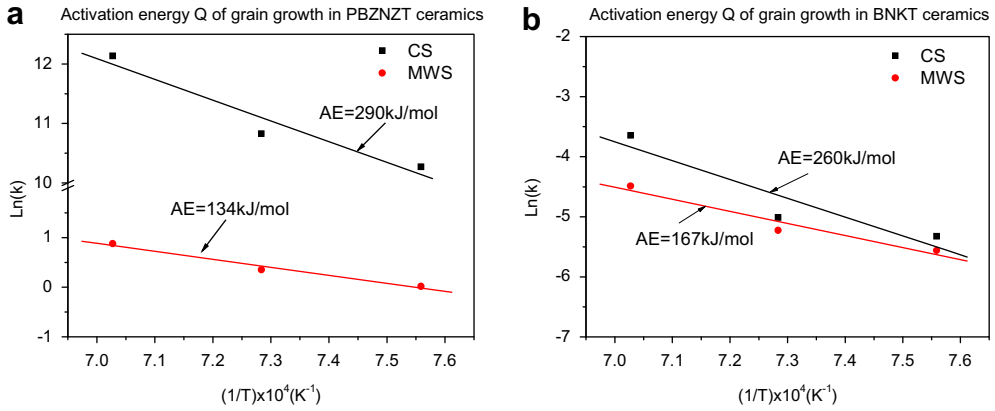

Fig. 7. Activation energy of grain growth for (a) PBZNZT samples and (b) BNKT samples sintered in conventional and microwave furnaces.

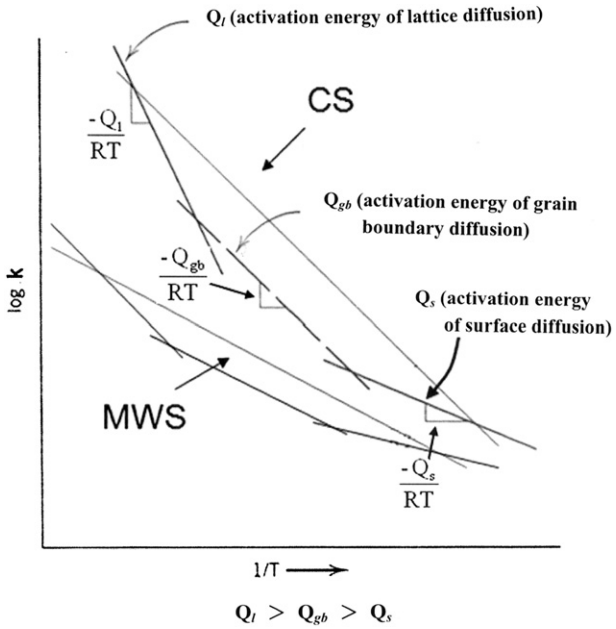

Fig. 8. Schematic diagram of the average activation energy of mass transport compared with CS and MWS sintering.

powders to prevent the evaporation of Bi_2O_3, Na_2O, and K_2O. All specimens had been polished to a thickness of 0.6 mm, and a silver paste was applied as the electrodes and baked at 650 °C for 30 min to facilitate electrical measurements. Fig. 1 displays the experimental schematic diagram of the MWS process and the temperature profiles of the MWS and the CS processes. X-ray diffraction (XRD) technique (Rigaku, Max-RC, Japan) was used to determine the crystal phase of the samples. Micrographs of the prepared samples were obtained using a scanning electron microscope (SEM; JEOL FESEM 6500F). The chemical homogeneity of the specimens was investigated using an energy-dispersive spectrometer (EDS) attached to a transmission electron microscope with a field emission gun (FEG-TEM; Tecnai G^2 F20). The density was measured using the Archimedes method with distilled water. The P–E hysteresis loops were obtained by a Sawyer–Tower circuit. The temperature dependence of the dielectric properties was evaluated using a network analyzer (Agilent E5071C) from room temperature to 430 °C at a frequency of 2.45 GHz. A Solartron 1260 AC impedance analyzer was used to measure the impedance plots between 400 °C and 700 °C in the frequency range of 0.1 Hz–5 GHz. The piezoelectric planar coupling coefficient (kp) was determined by the resonance–anti resonance method using a HP 4194A.

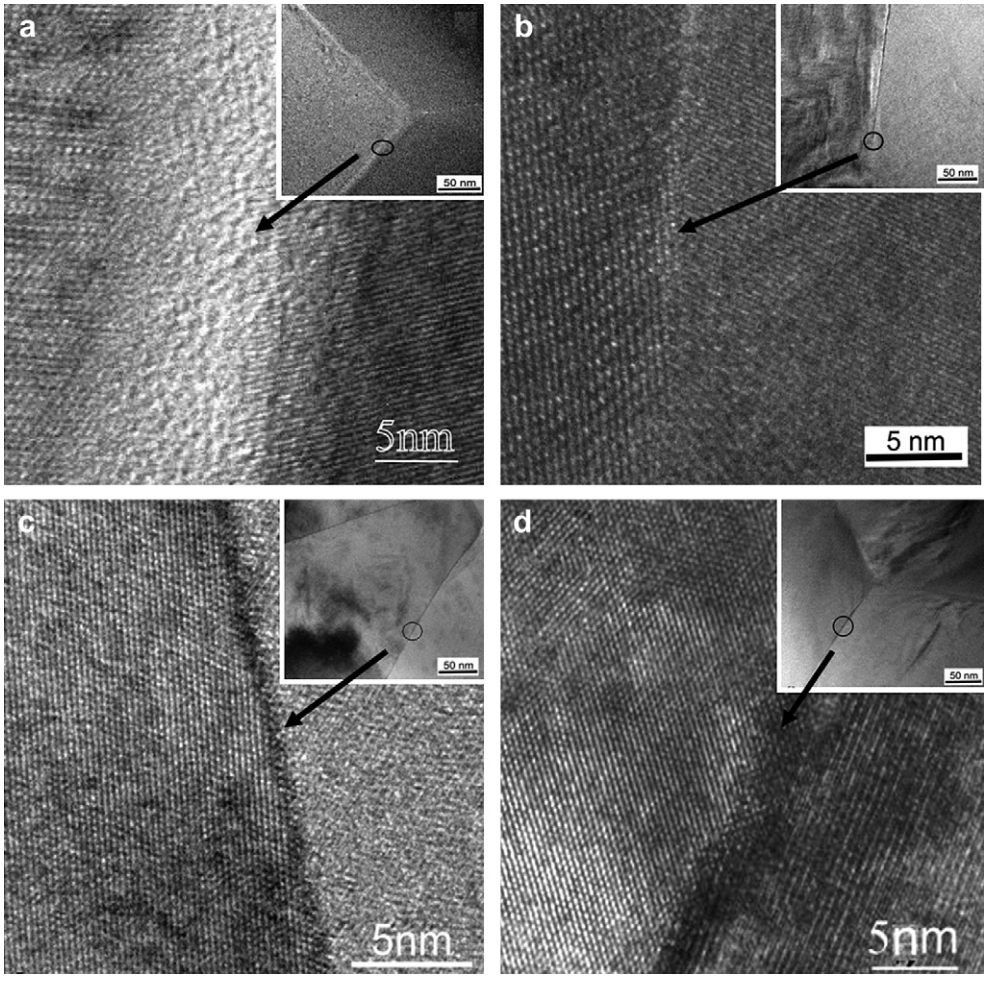

Fig. 9. HRTEM atomic structure images of grain boundaries for PBZNZT samples using (a) CS (b) MWS process and BNKT samples using (c) CS (d) MWS process.

3. Results and discussion

The relative theoretical densities of PBZNZT and BNKT specimens sintered using the CS and MWS processes are displayed in Fig. 2. The relative density of sintered PBZNZT samples increased as sintering temperature increased for the CS process and the relative density initially increased and then decreased for the MWS process. A comparison between CS specimens sintered at 1150 °C for 2 h and MWS specimens sintered at 1050 °C for 2 h, at a similar density, indicated that the MWS process could achieve a significantly lower sintering temperature in PBZNZT samples for the same densification. This result implied that the PBZNZT specimens absorbed microwave radiation more efficiently during sintering. On the other hand, BNKT specimens achieved a similar density for CS and MWS specimens demanding the same sintering temperature at 1150 °C for 2 h. The result indicates that BNKT samples appear to display less microwave absorption ability. At the same time, the relative density of PBZNZT specimens sintered at 1150 °C for 10 min in the MWS process could reach 98%. However, BNKT specimens used the MWS process to achieve a relative density of 98% requiring a soaking time of 2 h at 1150 °C. The PBZNZT specimens obviously displayed a higher microwave absorption ability. To understand microwave absorption ability, the dielectric constants and dielectric loss of both PBZNZT and BNKT specimens in the MWS process were evaluated. The dielectric constants and dielectric loss were measured as functions of temperature at a frequency of 2.45 GHz from the temperatures range of 25 to 400 °C as shown in Fig. 3. The maximum dielectric constant, ε_{max}, is approximately 2200 for PBZNZT specimens sintered at 1150 °C for 10 min, and 1000 for the BNKT specimens sintered at 1150 °C for 2 h. The dielectric constant of PBZNZT samples was around double that of BNKT samples. On the other hand, the dielectric loss factor of PBZNZT specimens also displayed a higher value than that of the BNKT specimens within the same range of measured temperatures. The dielectric loss factor involves the conduction loss and the dipole loss. For microwave sintering, ferroelectric and piezoelectric materials can couple microwave energy through conduction loss and dipole loss. This allows them to be heated more efficiently in the microwave field. A higher dielectric constant accompanies a larger dielectric loss, leading to a larger absorption of microwave energy in PBZNZT specimens. To evaluate the conduction loss or the dipole loss from the dielectric loss, which plays the main role in the microwave absorption, AC impedance measurements were performed on the BNKT and PBZNZT specimens sintered using the MWS process. The AC impedance measurements were performed in the frequency range of 0.1 Hz to 5 GHz in the temperature range of 400–700 °C. Fig. 4 displays the impedance spectroscopic plots and the semicircle arcs that were observed in the temperature range of 400 °C to 700 °C, and these plots show the different semicircle arcs at different temperatures. This means that different conductivities exist at different temperatures. The radius of the semicircle gives the resistance of the material. To calculate the conductivity of the total bulk, the bulk resistance (R_{bulk}) is obtained from the interception of the semicircle with the real axis (Z') in the complex plots. The value of R_{bulk} at each test temperature was converted into the bulk conductivity (σ_{bulk}) by the relation:

$$\sigma = t/SR \tag{2}$$

where t is the sample thickness and S is the electrode area on the sample surface. The conductivity changes with temperature for PBZNZT and BNKT samples sintered using the microwave process shown in Fig. 5. According to the characteristic frequency of complex impedance, the conduction loss can be calculated by the relation:

$$\varepsilon_c'' = \frac{\sigma}{\omega\varepsilon_0} \tag{3}$$

where ε_c is the conduction loss, ε_0 is the permittivity of free space; ω is the characteristic frequency of the specimen, and σ is the

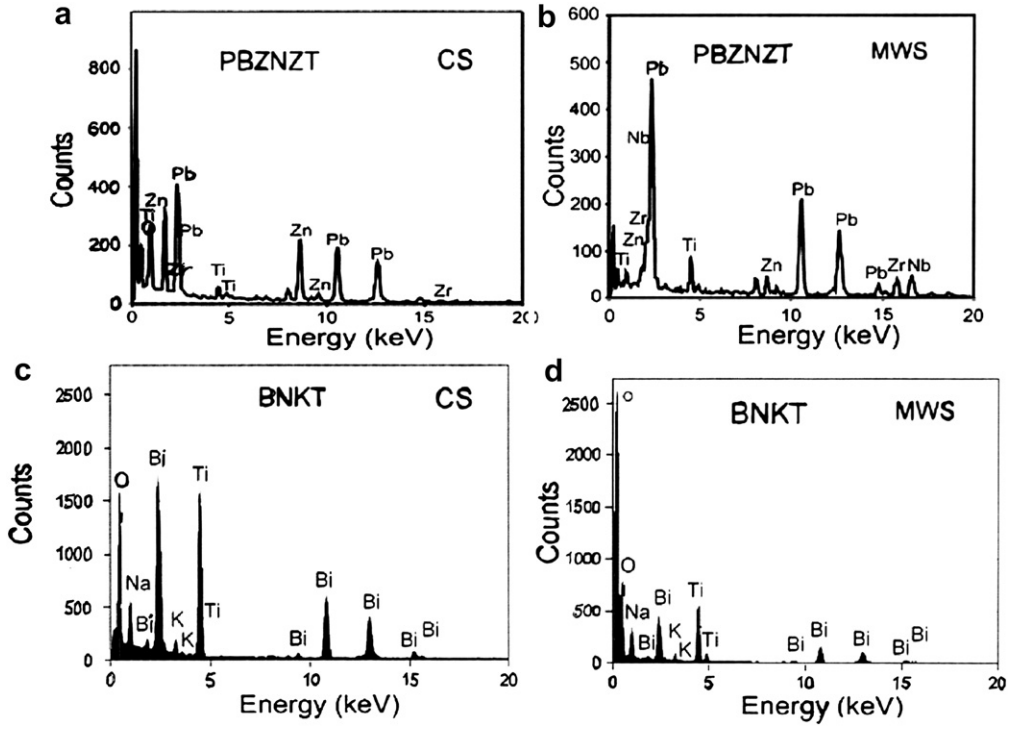

Fig. 10. EDS spectra of a grain boundary in PBZNZT specimens for (a) CS (b) MWS processes and in BNKT specimens for (c) CS (d) MWS processes.

Table 1
TEM–EDS elemental analyses of grain boundaries for PBZNZT and BNKT samples.

(unit: at.%)					
	Pb	Ti	Zn	Zr	Nb
PBZNZT (CS process)	44.8	7.2	44.6	1.9	1.6
PBZNZT(MWS process)	47.6	15.6	8.0	12.8	16.1
	Bi	Na	K	Ti	O
BNKT (CS process)	16.6	9.8	0.8	16.5	56.4
BNKT (MWS process)	8.0	11.5	0.9	17.0	62.2

conductivity. To provide a concrete explanation, the data of complex impedance and dielectric loss at 400 °C are given an example. The dielectric loss of PBZNZT ceramics is 0.10113 and that of BNKT ceramics is 0.00663. At the same time, the conductivity of PBZNZT ceramics is calculated by Eq. (2), and the result of the conductivity is substituted into Eq. (3) to calculate the conduction loss. Therefore, the conduction losses of PBZNZT and BNKT ceramics at 400 °C are 0.00045 and 0.00068, respectively. This result indicates that the BNKT specimens display higher conduction losses. This may be because vapor pressure of bismuth oxide is higher than that of lead oxide [35], implying that bismuth oxide in BNKT ceramics more easily vaporizes compared with lead oxide in PBZNZT ceramics. Because the dipole loss can be calculated by subtracting conduction loss from the dielectric loss, the values of the dipole losses in PBZNZT and BNKT ceramics at 400 °C will be 0.10065 and 0.00592, respectively. According to the above interpretation, PBZNZT showed a higher dipole loss and a similar conduction loss, but displayed higher microwave absorption. The results might be attributed to the contribution of dielectric constant and dipole loss. Therefore, dielectric properties might dominate the microwave absorption ability for ferroelectric and piezoelectric materials.

The grain sizes of PBZNZT and BNKT specimens sintered using the CS and MWS processes were measured and the grain size of PBZNZT specimens in the MWS process was smaller than that of in the CS process for similar relative density. The grain size of MWS samples was 1.72 μm at a sintering temperature of 1050 °C for 2 h and of the CS samples was 2.1 μm at a sintering temperature of 1150 °C for 2 h. Moreover, the grain sizes of the MWS and CS specimens in BNKT specimens were also evaluated and the results indicated that the grain size of the MWS process was also smaller for the similar relative densities of the CS and MWS samples. The grain size of the MWS process is 1.11 μm at 1150 °C for 2 h and that of CS process is 1.47 μm at 1150 °C for 2 h. The SEM images of PBZNZT and BNKT specimens are shown in Fig. 6, and obviously exhibit a smaller grain size for the MWS process than for the CS process. According to M.A. Janney [22], the surface diffusion at the lower sintering temperature is the main diffusion mechanism of grain coarsening, whereas the grain boundary and bulk diffusions at higher sintering temperature are the main diffusion mechanism of densification. The microwave sintering process was observed to densify PBZNZT and BNKT materials with no induced surface diffusion of coarsening grain due to a very rapid rate of heating that enhanced grain boundary and bulk diffusions of rapid densification resulting in high-density materials containing a finer grain microstructure.

The activation energy for the grain growth was calculated by the grain growth kinetics equation:

$$G^n - G_0^n = K_0 t \exp(-Q/RT) \quad (4)$$

where G is grain size, G_0 is initial grain size, K_0 is the grain growth rate constant, t is sintering time, n is the grain growth kinetic exponent, Q is the activation energy of grain growth, R is gas constant, and T is sintering temperature. The activation energy of BNKT ceramics in microwave sintered sample is lower (167 kJ/mol) than that of conventional one (260 kJ/mol). On the other hand, the

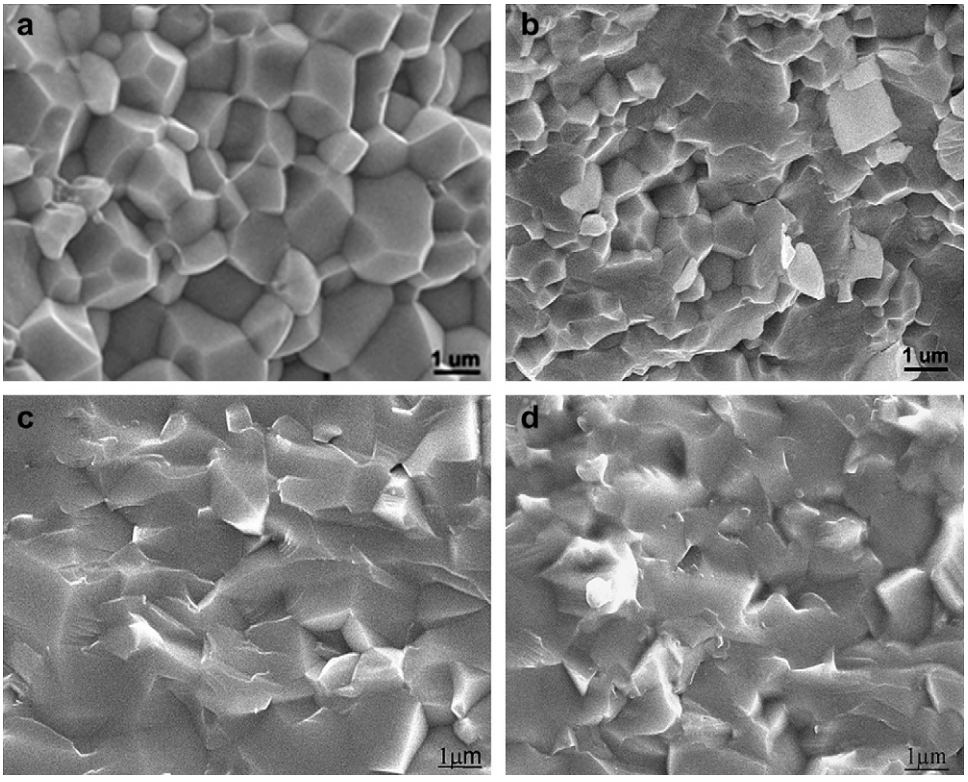

Fig. 11. SEM images of fracture surface for (a) PBZNZT samples and (b) BNKT samples using microwave sintering.

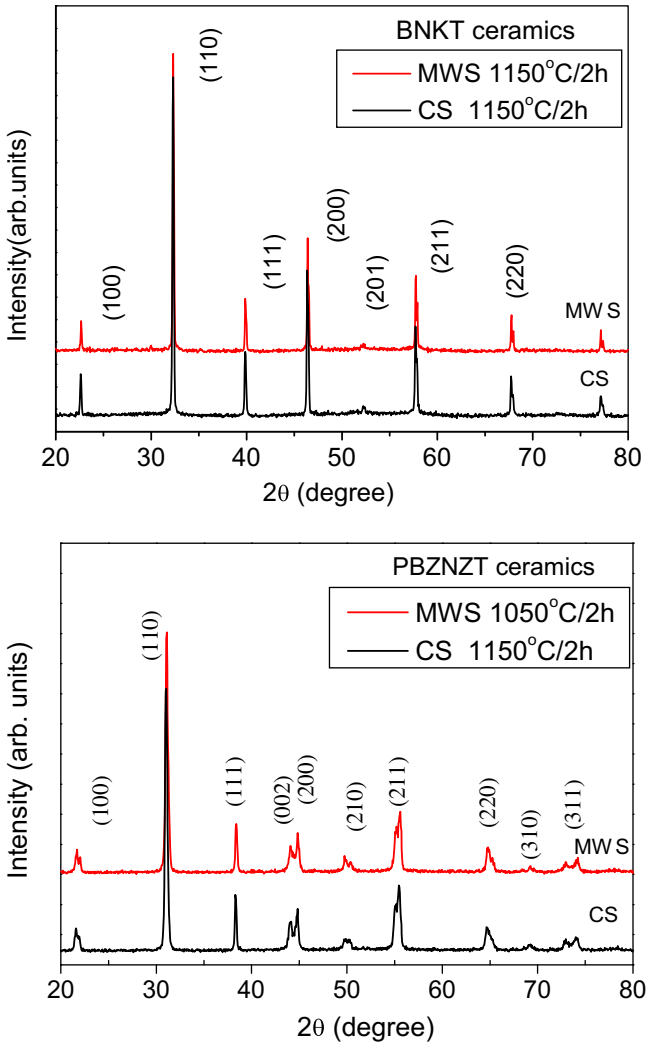

Fig. 12. X-ray diffraction patterns of BNKT and PBZNZT specimens sintered using the CS and MWS processes.

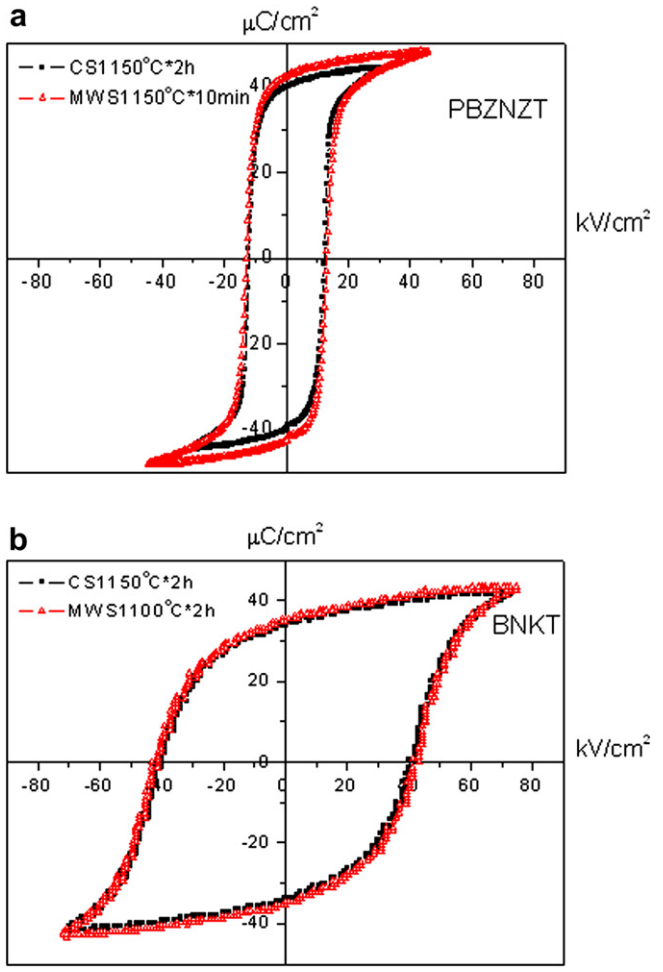

Fig. 13. *P–E* hysteresis loops of (a) PBZNZT and (b) BNKT specimens using conventional and microwave sintering.

activation energy of PBZNZT ceramics in microwave sintered sample is also lower (132 kJ/mol) than that of the conventional one (238 kJ/mol) as shown in Fig. 7. The results indicate that MWS process displays lower activation energy for PBZNZT and BNKT specimens. To compare the difference between MWS and CS in the sintering mechanism of mass transport, Fig. 8 displays the schematic diagram for the average activation energy of mass transport in the CS and MWS sintering. The activation energy calculated by the grain growth kinetics equation represents the average value of the activation energy of surface diffusion, grain boundary diffusion, and volume diffusion. The existence of lower activation energy in the specimens of MWS process implies that lower values of activation energies of surface diffusion, grain boundary diffusion, and volume diffusion exists in the specimens of MWS process. This means that microwave radiation enhances atomic diffusion and aids sintering behavior of PBZNZT and BNKT ceramics.

To compare the difference between the microstructures and the electrical properties of PBZNZT and BNKT ceramics in the CS and MWS processes, we utilized electron microscopy to explore the correlation between electrical properties and microstructures. TEM was performed to investigate the microstructure characteristics of the specimens. Fig. 9 displays the high resolution electron microscopy images of grain boundaries in PBZNZT and BNKT specimens. The images of PBZNZT specimens for CS process exhibit an obvious amorphous phase at the grain boundaries shown in Fig. 9(a). It was reported that PbO might segregate to form the amorphous layer or second phases [36–38]. A semi-quantitative TEM-EDS study of the grain boundary showed that grain boundaries possess more PbO and ZnO as shown in Fig. 10(a) and Table 1. Therefore, not only PbO but also ZnO form the intergranular layer with a thickness of about 10 nm in the present PBZNZT material system. Meanwhile, SEM observations of the fracture surface revealed an obvious and continuous intergranular type of fracture, as shown in Fig. 11(a). This result corresponds to weaker bonds and a continuous phase existing at the grain boundaries, which can be attributed to the segregation of the amorphous phase at the grain boundaries. On the other hand, the MWS specimen exhibited a thin grain boundary with a thickness less than 1 nm, as observed in Fig. 9(b) and the TEM-EDS displayed an ordinary concentration gradient as shown in Fig. 10(b) and Table 1. The composition analysis at the grain boundary is also similar to that of the grain interior. SEM observations of the fracture surface display a transgranular type of fracture, as shown in Fig. 11(b). The results suggest that the volatile elements such as PbO and ZnO segregating at the grain boundaries are less in the MWS process, which produces better crystallization and fewer defects in the materials.

TEM images of BNKT specimens can be seen in Fig. 9(c) and (d). The BNKT specimens for the CS and MWS process display a clean atomic arrangement at the grain boundaries. At the same time,

Table 2
Ferroelectric properties and electromechanical coupling factor *kp* of conventional and microwave sintered PBZNZT and BNKT specimens.

	CS			MWS		
	Pr	Ec	kp	Pr	Ec	kp
PBZNZT	41.6	13.10	0.54	38.9	13.15	0.60
BNKT	34.2	40.60	0.28	35.3	42.05	0.30

a thin grain boundary with a thickness of less than 1 nm was observed. The compositional analysis of the TEM-EDS at the grain boundaries is shown in Fig. 10(c) and (d) and in Table 1, and the results are similar to those of the grain interior. However, MWS specimens display a less stoichiometric deviation than CS specimens. This may be the reason why MWS specimens display higher electrical properties than CS specimens. On the other hand, SEM observations of the fracture surface revealed a transgranular type of fracture for CS and MWS specimens, as shown in Fig. 11(c) and (d). This implies the existence of stronger bonds at the grain boundaries for BNKT specimens. This result is different from PBZNZT ceramics with a continuous amorphous layer at the grain boundaries.

X-ray diffraction patterns for conventional and microwave sintered PBZNZT and BNKT specimens are shown in Fig. 12. Characteristic peaks in the X-ray diffraction pattern of sintered specimens indicate the formation of a perovskite structure. The pyrochlore phase formed very easily in the PZN material system. The PBZNZT ceramics use an ASMC method, which efficiently reduces pyrochlore phase generation. On the other hand, the patterns of BNKT ceramics primarily exhibit the perovskite structure. These results are shown in Fig. 12. Compared to the crystal structure of PBZNZT and BNKT sintered specimens, the c/a ratios of the tetragonal phases in the CS and MWS processes for PBZNZT specimens are 1.013 Å and 1.016 Å, respectively and for BNKT specimens are 1.0062 Å and 1.0069 Å, respectively. The MWS process obviously displays a larger tetragonality for PBZNZT and BNKT specimens.

To understand the effects of the CS and MWS processes on the electrical properties, the ferroelectric and piezoelectric properties were measured. Fig. 13 shows typical hysteresis loops obtained in PBZNZT and BNKT specimens sintered by conventional and microwave processes. For PBZNZT specimens at a similar density, the remnant polarization value (P_r) of CS samples sintered at 1150 °C for 2 h is 38.9 μC/cm^2 and the value is 41.6 μC/cm^2 for MWS samples sintered at 1150 °C for 10 min. For BNKT specimens, the P_r value is 34.2 μC/cm^2 for the CS samples sintered at 1150 °C for 2 h and the value increases to 35.3 μC/cm^2 for the MWS samples sintered at 1150 °C for 2 h. On the other hand, the coercive field becomes smaller in the MWS process for BNKT and PBZNZT specimens. These ferroelectric property parameters are listed in Table 2. The values of the planar electromechanical coupling factor, *kp* were measured and calculated. In PBZNZT ceramics, the value of *kp* is 0.54 for CS specimens sintered at 1150 °C for 2 h and the value is 0.6 for MWS specimens sintered at 1150 °C for 10 min. On the other hand, BNKT specimens indicate that the *kp* is 0.28 for CS specimens sintered at 1150 °C for 2 h and the value is 0.3 for MWS specimens sintered at 1150 °C for 2 h. The results are also listed in Table 2 and the electrical properties of the MWS samples are higher, suggesting that MWS samples possess fewer defects and better crystallization.

4. Conclusions

The microwave sintering process has been successfully performed on PBZNZT and BNKT piezoelectric ceramics. The results indicate that the grain sizes of the MWS process for PBZNZT and BNKT specimens are smaller than these of the CS process for the same densification, and PBZNZT samples could achieve a significantly lower sintering temperature in the MWS process, implying that PBZNZT specimens absorb microwave radiation more efficiently. This could be attributed to the contribution of the dielectric constant and dipole loss. Therefore, the dielectric properties might dominate the microwave absorption ability of ferroelectric and piezoelectric materials.

HRTEM and energy dispersive spectroscopic investigations show that the grain boundaries of MW samples exhibit less PbO and ZnO segregation than those of the CS samples for PBZNZT specimens. The BNKT specimens display no compositional segregation at grain boundaries for the CS and MWS processes. However, the MWS process could efficiently achieve a more uniform composition and crystallization for PBZNZT and BNKT ceramics, and the results improve the electrical properties.

Acknowledgements

The authors acknowledge the financial support by the National Science Council of Taiwan for the project No: 97-2923-M-029-001-MY3 & 99-2218-E-131-003.

References

[1] N. Vittayakorn, G. Rujijanagul, T. Tunkasiri, X. Tan, D.P. Cann, J. Mater. Res. 18 (2003) 2882.
[2] H. Fan, H.E. Kim, J. Appl. Phys. 91 (2002) 317.
[3] N. Vittayakorn, G. Rujijanagul, X. Tan, H. He, M.A. Marquardt, D.P. Cann, J. Electroceram. 16 (2006) 141.
[4] S.Y. Chen, C.M. Wang, S.Y. Cheng, Mater. Chem. Phys. 52 (1998) 207–213.
[5] A. Halliyal, U. Kumar, R.E. Newnham, L.E. Cross, J. Am. Ceram. Soc. 70 (1987) 119.
[6] J.R. Belsick, A. Halliyal, U. Kumar, R.E. Newnham, Am. Ceram. Soc. Bull. 66 (1987) 664.
[7] T. Takenaka, H. Nagata, J. Eur. Ceram. Soc. 25 (2005) 2693.
[8] T. Takenaka, K. Maruyama, K. Sakata, Jpn. J. Appl. Phys. 30 (9B) (1991) 2236.
[9] T. Takenaka, K. Sakata, Ferroelectrics 95 (1989) 153.
[10] H. Nagata, T. Takenaka, Jpn. J. Appl. Phys. 36 (1997) 6055.
[11] A. Sasaki, T. Chiba, Y. Mamiya, E. Otsuki, Jpn. J. Appl. Phys. 38 (1999) 5564.
[12] L. Wu, D. Xiao, Jpn. J. Appl. Phys. 46 (11) (2007) 7382.
[13] Y. Hiruma, K. Yoshii, J. Appl. Phys. 103 (2008) 084121.
[14] Y. Hiruma, H. Nagata, T. Takenaka, Jpn. J. Appl. Phys. 45 (9B) (2006) 7409.
[15] G. Fan, W. Lu, Appl. Phys. Lett. 91 (20) (2007) 202908.
[16] Y. Yao, Y. Tseng, J. Appl. Phys. 102 (2007) 094102.
[17] C.W. Tai, S.H. Choy, J. Am. Ceram. Soc. 91 (10) (2008) 3335.
[18] R. Zuo, S. Su, Mater. Chem. Phys. 110 (2–3) (2008) 311.
[19] C.C. Chou, H.Y. Chang, I.N. Lin, B.J. Shaw, J.T. Tan, Microscopic examination of the microwave sintered $(Pb_{0.6}Sr_{0.4})TiO_3$ positive temperature coefficient resistor materials, Jpn. J. Appl. Phys. 37 (1998) 5269–5272.
[20] C.L. Li, M.B. Suresh, C.C. Chou, High-K dielectric PZN-based materials prepared by microwave sintering for reduction of defects, J. Phys. Chem. Solids 69 (2008) 611–615.
[21] A.C. Metaxas, J.G.P. Binner, Microwave processing of ceramics. in: J.G.P. Binner (Ed.), Advanced Ceramic Processing Technology. Noyes Publications, New Jersey, USA, 1990, pp. 285–367.
[22] M.A. Janney, H.D. Kimeey, Diffusion -controlled processes in microwave fired oxide ceramics. in: W.B. Snyder Jr., W.H. Sutton, M.F. Iskander, D.L. Johnson (Eds.), Microwave Processing of Materials II, Materials Research Society Symposium Proceedings, vol. 189. Materials Research Society, Pittsburgh, PA, 1991, pp. 215–227.
[23] F. Selmi, F. Guerin, X.D. Yu, V.K. Varadan, S. Komarneni, Microwave calcination and sintering of barium strontium titanate, Mater. Lett. 12 (1992) 424.
[24] Z. Xie, J. Yang, X. Huang, Y. Huang, Microwave processing and properties of ceramics with different dielectric loss, J. Eur. Ceram. Soc. 19 (1999) 381–387.
[25] A. Goldstein, M. Kravchik, Sintering of PZT powders in MW furnace at 2.45 GHz, J. Eur. Ceram. Soc. 19 (1999) 989–992.
[26] W.B. Harrison, M.R.B. Hanson, B.G. Koepke, Microwave processing and sintering of PZT and PLZT ceramics, Mater. Res. Soc. Symp. Proc. 124 (1988) 279–286.
[27] H. Takahashi, K. Kato, Q. Jinhao, T. Junji, Property of lead zirconate titanate actuator manufactured with microwave sintering process, Jpn. J. Appl. Phys. 40 (2001) 724–727.
[28] S. Rhee, D. Agrawal, T. Shrout, M. Thumm, Investigation of high microwave frequency (2.45 GHz, 30 GHz) sintering for Pb-based ferroelectrics and microscale functional devices, Ferroelectrics 261 (2001) 15–20.

[29] S. Rhee, T.R. Shrout, T.A. Ritter, M. Thumm, Investigation of high frequency (2.45 GHz, 30 GHz) processing of Pb-based piezoelectric for ultrasound transducers, IEEE Ultrason. Symp. 2 (2000) 981–984.
[30] C.C. Chou, P.H. Chen, I.N. Lin, Microstructural characteristics of microwave sintered semi-conductive Pb0.6Sr0.4TiO3 ceramics, Ferroelectrics 231 (1999) 37–42.
[31] P.H. Chen, H.C. Pan, C.C. Chou, I.N. Lin, Microstructures and properties of semiconductive (Pb0.6Sr0.4)TiO3 ceramics using PbTiO3-coated SrTiO3 p.wders, J. Eur. Ceram. Soc. 21 (2001) 1905–1908.
[32] W.H. Sutton, Microwave processing of ceramic materials, Am. Ceram. Soc. Bull. 68 (21) (1989) 376–386.
[33] C.L. Li, C.C. Chou, Integr. Ferroelectr. 50 (2003) 1549.
[34] C.L. Li, C.C. Chou, J. Eur. Ceram. Soc. 26 (2006) 1237.
[35] Y. Wu, G. Caoa, Appl. Phys. Lett. 75 (17) (1999) 2650.
[36] B.M. Song, D.Y. Kim, S.I. Shirasaki, H. Yamamura, Effect of excess PbO on the densification of PLZT ceramics, J. Am. Ceram. Soc. 72 (1989) 833–836.
[37] H.M. Jang, K.M. Lee, Stabilization of Pb(ZnMg)1/3Nb2/3 O3–0.045PbTiO3 p.rovskite phase and dielectric properties of ceramics prepared by excess constituent oxides, J. Mater. Res. 9 (1994) 2634–2644.
[38] M. Villegas, J.F. Fernandez, A.C. Caballero, Z. Samardija, G. Drazic, M. Kosec, Effects of PbO excess in Pb(Mg1/3Nb2/3)O3–PbTiO3 ceramics: Part II. Microstructure development, J. Mater. Res. 14 (1999) 898–905.